Microsc. Microanal. Page 1 of 6
doi:10.1017/S1431927613012750

Microscopy AND Microanalysis

Microstructural Characterization of Long-Period Stacking Ordered Phases in $Mg_{97}Zn_1Y_2$ (at.%) Alloy

Xiaohong Shao,[1,2] Huajie Yang,[1,2] Jeff T.M. De Hosson,[2,*] and Xiuliang Ma[1,*]

[1]*Shenyang National Laboratory for Materials Science, Institute of Metal Research, Chinese Academy of Sciences, Shenyang 110016, China*
[2]*Department of Applied Physics, Zernike Institute for Advanced Materials and Materials innovation institute M2i, University of Groningen, Nijenborgh 4, 9747 AG Groningen, the Netherlands*

Abstract: Transmission electron microscopy characterization of two major long-period stacking ordered (LPSO) phases in Mg–Zn–Y alloy, i.e., 18R- and 14H-LPSO are reported. The space group and atomic-scale microstructures of both compounds were determined using a combination of electron diffraction, convergent beam electron diffraction, high-resolution transmission electron microscopy, and *Z*-contrast scanning transmission electron microscopy. The 18R-LPSO phase is demonstrated to have a point group and space group $3m$ and $R3m$ (or $\bar{3}m$ and $R\bar{3}m$), with the lattice parameter $a = 1.112$ nm and $c = 4.689$ nm in a hexagonal coordinate system. The 14H-LPSO phase has a point group $6/mmm$ and a space group $P6_3/mmc$, and the lattice parameter is $a = 1.112$ nm and $c = 3.647$ nm. In addition, insertion of extra thin Mg platelets of several atomic layers, results in stacking faults in the LPSO phase. These results may shed some new light on a better understanding of the microstructure and deformation mechanisms of LPSO phases in Mg alloys.

Key words: Mg–Zn–Y alloy, LPSO phase, space group, STEM

Introduction

Magnesium alloys have attracted increasing interest as lightweight structure materials owing to their low density, high specific strength, good damping, and ease of recycling, which can be used in many fields including automotive, tools, sports equipment, electronic equipment, and aerospace (Zhang et al., 2007*a*). However, the low strength and poor ductility of Mg alloys are critical issues and so far have strongly limited their widespread application. Adding alloy elements is one of the most effective methods to improve mechanical properties of Mg alloys (Inoue et al., 2001; Bae et al., 2002; Yamasaki et al., 2005; Honma et al., 2007).

$Mg_{97}Zn_1Y_2$ (at%) alloy exhibits high thermal stability and exceptional mechanical properties (Inoue et al., 2001; Kawamura et al., 2001), owing to a novel precipitate with long-period chemical and stacking ordered (LPSO) structure (Abe et al., 2002). Various LPSO phases of 10H, 14H, 18R, and 24R types LPSO have been observed in several kinds of ternary Mg–Zn–RE (rare earth) systems (Chino et al., 2004; Itoi et al., 2004; Matsuda et al., 2005; Kawamura & Yamasaki, 2007). It has been reported that LPSO phases play a significant role in strengthening and toughening Mg alloys, especially at high temperatures (Shao et al., 2010; Hagihara et al., 2013).

The LPSO structures in as-cast Mg–Zn–Y alloys were reported as a monoclinic 6H type in the beginning (Abe et al., 2002; Ping et al., 2002). Afterwards, 18R other than 6H was examined to describe the LPSO phase formed in as-cast state and rapid solidification process (Luo & Zhang, 2000; Itoi et al., 2004; Matsuda et al., 2005). The lattice parameter was $a = 0.321$ nm and $c = 4.86$ nm in hexagonal coordinates, with a stacking sequence of ABABABCACA CABCBCBCA along the [0001] direction (Luo & Zhang, 2000; Itoi et al., 2004; Matsuda et al., 2005). Meanwhile, the 14H-LPSO phase was identified as the major LPSO phase in Mg–Zn–RE alloy after suitable heat treatment (Yoshimoto et al., 2006; Kawamura & Yamasaki, 2007; Yamasaki et al., 2007; Zhu et al., 2007, 2010). The 14H-LPSO phase has a hexagonal lattice ($a = 0.325$ nm and $c = 3.694$ nm), with a stacking sequence of ACBCBABABABCBC along the [0001] direction (Matsuda et al., 2005). In addition, other stacking sequences have also been reported, e.g. ABABABACACA CAC (Amiya et al., 2003) and ABACBCBCBCABAB (Matsuura et al., 2006). Recently, Zhu et al. (2007, 2010) provided a new result of 18R- and 14H-LPSO structures in Mg–Y–Zn alloys. 18R-LPSO structure has an ordered base-centered monoclinic lattice ($a = 1.112$ nm, $b = 1.926$ nm, $c = 4.689$ nm, $\beta = 83.25°$), with Y and Zn atoms having an ordered arrangement in the close-packed planes. Furthermore, the composition of 18R is suggested to be $Mg_{10}Y_1Zn_1$, instead of the $Mg_{12}Y_1Zn_1$ composition that is commonly accepted (Luo & Zhang, 2000). The 14H has a hexagonal unit cell ($a = 1.112$ nm, $c = 3.647$ nm) and the ordered distribution of Y and Zn atoms in the unit cell is similar to that in the 18R and its composition is $Mg_{12}Y_1Z_1$. A fully crystal characterization of LPSO structures may result in a further understanding of microstructures and deformation mechanisms of LPSO phases in Mg alloys.

A combination of electron diffraction pattern (EDP) and convergent beam electron diffraction (CBED) was successfully applied in determining the symmetry of ternary

Received February 4, 2013; accepted June 17, 2013
*Corresponding authors. E-mail: J.T.M.De.Hosson@rug.nl, xlma@imr.ac.cn

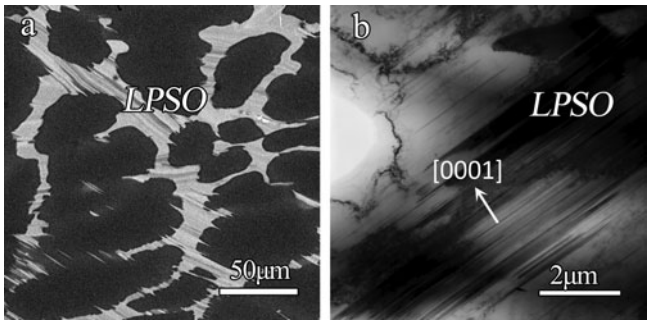

Figure 1. a: A BSE-SEM image showing the general characteristics of the microstructures in as-cast $Mg_{97}Zn_1Y_2$ (at.%) alloy; (**b**) low-magnification TEM image exhibiting salient features of the LPSO phase.

carbides such as Ti_3AlC_2 (Ma et al., 2004) and Zr–Al–C (Lin et al., 2006). Therefore, in this work these two methods were employed to identify the symmetry of the LPSO phase in Mg–Zn–Y alloys. It should provide more precise information about the space group. We report the detailed microstructural characterization of LPSO structures in $Mg_{97}Zn_1Y_2$ (at%) alloy via transmission electron microscopy (TEM). The symmetry of both 18R- and 14H-LPSO phases was determined using a combination of EDP and CBED. Atomic-scale microstructures were achieved by means of high-resolution TEM (HRTEM) and *Z*-contrast scanning transmission electron microscopy (STEM).

Materials and Methods

Samples with a nominal composition of $Mg_{97}Zn_1Y_2$ (at.%) were prepared from high purity Mg, Zn, and Mg–25Y (wt%) master alloy by high-frequency induction melting in a graphite crucible at ~750°C under an argon atmosphere. The heat treatment samples were solution treated at 500°C for 5 h sealed in a quartz tube in an Ar atmosphere in order to avoid Mg alloy oxidation. Both samples at cast state and after heat treatment were observed using a LEO supra 35 scanning electron microscope (SEM) and TEM. Thin foil samples for TEM were prepared by conventional ion-milling methods. A 200 kV JEOL-2100 TEM was used for EDP and CBED analysis. A 300 kV Tecnai G^2 F30 TEM, equipped with an HAADF detector, was used for high-resolution imaging and *Z*-contrast STEM imaging. Fast Fourier transformation (FFT) was carried out using a Digital Micrograph software package.

Results and Discussion

Figure 1a shows a BSE-SEM image exhibiting general characteristics of the microstructures present in the as-cast $Mg_{97}Zn_1Y_2$ (at.%) alloy. The LPSO phase with 5–35 μm in thickness results in a three-dimensional dendritic microstructure in the Mg alloy. Figure 1b is a low-magnification TEM image of the LPSO phase. When imaged along the $[hki0]$ direction of Mg matrix, the LPSO phase shows parallel fringes along the [0001] direction. Statistical analysis on 20

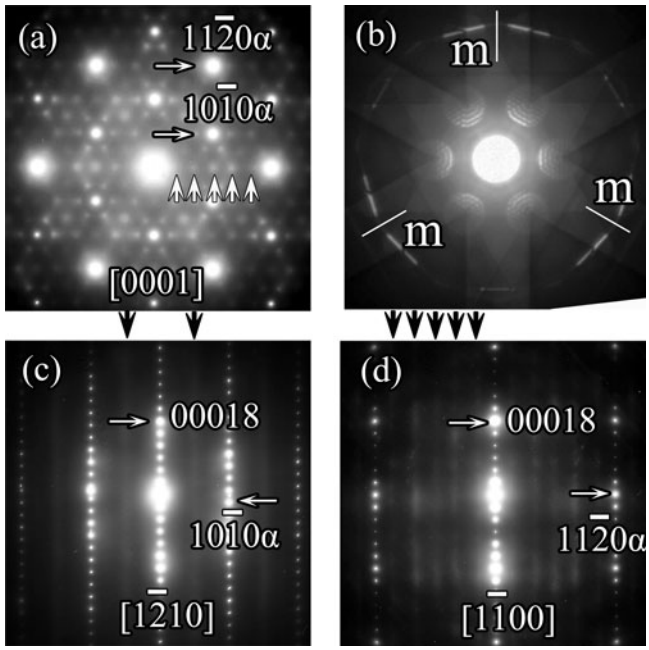

Figure 2. a: Selected-area electron diffraction (SAED) pattern of the 18R-LPSO phase recorded along the [0001] direction. **b:** A corresponding CBED pattern along the [0001] zone axis, showing the symmetry of a threefold rotation about the [0001] axis and also the symmetry of the mirror reflection across the $(1\bar{2}10)$ plane. **c, d:** SAED patterns of the 18R-LPSO phase with the electron beam parallel to the zone axis of $[1\bar{2}10]$ and $[1\bar{1}00]$, respectively.

EDX spectra shows that composition of the 18R-LPSO phase is Mg:Zn:Y = (83.2 ± 1.0):(8.7 ± 0.9):(8.1 ± 1.2). It has been reported that the 18R-LPSO phase is the dominant LPSO phase in $Mg_{97}Zn_1Y_2$ (at.%) alloys at the as-cast state (Itoi et al., 2004; Matsuda et al., 2005; Kawamura & Yamasaki, 2007; Ono et al., 2008; Zhu et al., 2009).

EDPs of the 18R-LPSO phase are displayed in Figure 2. The $[0001]_\alpha$ pattern in Figure 2a obviously shows that there are five additional reflections at positions of $1/6\{11\bar{2}0\}_\alpha$, $1/3\{11\bar{2}0\}_\alpha$, $1/2\{11\bar{2}0\}_\alpha$, $2/3\{11\bar{2}0\}_\alpha$, $5/6\{11\bar{2}0\}_\alpha$, respectively, and another extra spot at position $1/2\{11\bar{2}0\}_\alpha$. Figure 2b is a corresponding CBED pattern recorded along the [0001] zone axis. There is a threefold axis of rotational symmetry, as well as a mirror plane (which is reproduced every 120° by the action of the threefold axis). Combining the EDP pattern (Fig. 2a) and CBED pattern (Fig. 2b), it is clear that the symmetry along the [0001] zone axis is $3m$. Referring to the international tables for crystallography (Hahn et al., 1983), the symmetry of $3m$ along the $[0001]_\alpha$ zone axis and the reflection conditions of $h\bar{h}0l$: $h + l = 3n$, $hh\bar{2}\bar{h}l$: $l = 3n$ correspond to point group and space groups: $3m$ and $R3m$; $\bar{3}m$ and $R\bar{3}m$, respectively. Moreover, it is seen that there is one higher-order Laue zones in Figure 2b. When the electron beam passes exactly along the $[uvw]$ direction in the crystal, the radius of the center of the Laue zones, *R*, is approximately given by (Hirsch, 1977):

$$R = \lambda L(2Nd'/\lambda)^{1/2}, \quad (1)$$

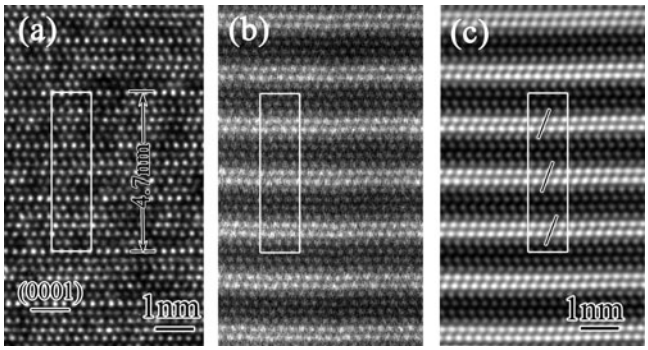

Figure 3. High-resolution (**a**) TEM and (**b**) *Z*-contrast STEM images of the 18R-LPSO phase recorded with the incident beam parallel to the $[1\bar{2}10]$ direction. **c**: Fast Fourier transformation filtered image of (**b**). These images clearly show the stacking sequence and the layers enriched with Zn/Y elements of the 18R-LPSO phase.

where λL is the diffraction constant, N is an integer that indicates the order of the Laue zone, d' is the spacing of the (uvw) reciprocal lattice plane, and λ is the electron wavelength. d' was calculated to be about 4.72 nm from the first-order Laue zones in Figure 2b when the electron beam is parallel to the [0001] direction, suggesting that the lattice parameter c is about 4.72 nm.

From the $[1\bar{2}10]_\alpha$ pattern shown in Figure 2c, it can be observed that five extra diffraction spots are present at positions of $n/6$ (where n is an integer) of the $(0002)_\alpha$ diffraction. In addition, there are weak but still visible diffuse streaks (marked by arrows) along the $g(0002)_\alpha$ direction and at the $\pm 1/2\{1\bar{1}00\}_\alpha$ positions. Figure 2d shows the $[1\bar{1}00]_\alpha$ pattern, it should be noted that there are five diffuse streaks through $n/6\{11\bar{2}0\}_\alpha$ (where n is an integer, denoted by arrows) along the c^* direction, which is consistent with the results of the $[0001]_\alpha$ pattern shown in Figure 2a. Thus the EDPs (Fig. 2) can be indexed using a unit cell with hexagonal axes $a = 1.112$ nm and $c = 4.689$ nm (regarding the α-Mg-lattice $a_\alpha = 0.321$ nm and $c_\alpha = 0.521$ nm). The reflection conditions are summarized as follows:

$$hkil\text{: } -h + k + l = 3n,\ h\bar{h}0l\text{: } h + l = 3n,$$

$$hh\bar{2}\bar{h}l\text{: } l = 3n \text{ and } 000l\text{: } l = 3n.$$

Based on aforementioned analyses, the space group of the 18R-LPSO phase is $R3m$ or $R\bar{3}m$, and the lattice parameter is $a = 1.112$ nm and $c = 4.689$ nm.

Figure 3a is a HRTEM image of the 18R-LPSO recorded with the incident beam parallel to the $\langle 1\bar{2}10\rangle_{\text{LPSO}}$ direction, showing a stacking sequence of ABABCACACABCBCBCAB with a periodicity of 4.7 nm along [0001], where the underlined letters indicate the fcc stacking units. Figure 3b is an HR-STEM image of the 18R-LPSO phase and Figure 3c is an FFT-filtered image of Figure 3b, respectively. These demonstrate the heavier Zn and/or Y atoms distributed periodically at two middle layers of FCC units, denoted by BC, AB, and CA, in the 18R-LPSO phase viewing from the $\langle 11\bar{2}0\rangle_{\text{LPSO}}$

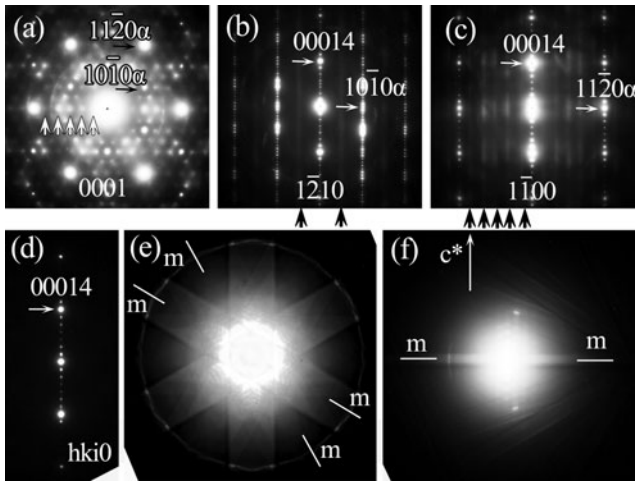

Figure 4. a–c: Selected-area electron diffraction (SAED) patterns of 14H-LPSO indexed as [0001], $[1\bar{2}10]$, and $[1\bar{1}00]$, respectively. **d:** An EDP, the orientation of which is positioned between $[1\bar{2}10]$ and $[1\bar{1}00]$. **e:** A CBED pattern showing the symmetry of a sixfold rotation about the [0001] axis and also the symmetry of the mirror reflection across the $(1\bar{2}10)$ and $(10\bar{1}0)$ planes. **f:** A CBED pattern showing the existence of a mirror plane on (0001). A combination of the information derived from these EDP and CBED patterns indicates that 14H-LPSO has a point group of $6/mmm$ and a space group of $P63/mmc$.

direction (Abe et al., 2002; Ping et al., 2002; Zhu et al., 2009, 2010; Shao et al., 2010), since the intensity Z-contrast STEM image is approximately proportional to Z^2 (the square of atomic number) (Pennycook & Jesson, 1992) or more accurately to $Z^{1.8}$ (Mizutani et al., 2009). Thus 18R-LPSO phase consists of two Mg layers alternating with one FCC stacking unit.

Figures 4a–4c show EDPs of the hexagonal 14H-LPSO phase in $Mg_{97}Zn_1Y_2$ (at.%) alloy after being heated at 500°C for 5 h, which are indexed as [0001], $[1\bar{2}10]$, and $[1\bar{1}00]$, respectively. From these low-index basic zone axes, the lattice parameters can be derived as $a = 1.112$ nm and $c = 3.647$ nm, which is consistent with the data reported earlier (Zhu et al., 2007, 2010). These EDPs are also informative for determining the extinction rules. In the $[1\bar{2}10]$ EDP, all reflections appear, but, in $[1\bar{1}00]$ the $(000l)$ reflections with $l =$ odd are extinct, implying the existence of a c glide plane. Figure 4d shows an EDP whose orientation is positioned between $[1\bar{2}10]$ and $[1\bar{1}00]$. It can be seen from Figure 4d that the $(000l)$ reflections with $l =$ odd are also absent, indicating there is a 6_3 screw axis along the [0001] axis. The appearance of the $\{000l\}$ ($l =$ odd) reflections in the $[1\bar{2}10]$ pattern can be attributed to double diffraction (Ma et al., 2004). Figure 4e shows a CBED pattern obtained from a 14H-LPSO phase along the [0001] zone axis. A sixfold axis of rotational symmetry as well as two independent mirror planes (each of which is reproduced every 60° by the action of the sixfold axis) were observed. These two types of mirror planes are parallel to the sixfold axis. The symmetry was determined to be $6mm$. In addition, the symmetry shown in the EDP $[1\bar{2}10]$ pattern (Fig. 4b) was $2mm$. A

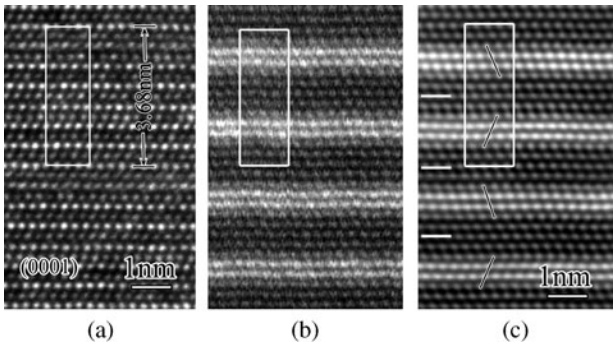

Figure 5. High-resolution (**a**) TEM and (**b**) *Z*-contrast STEM images of the 14H-LPSO phase recorded with the incident beam parallel to the $[1\bar{2}10]$ direction. **c**: Fast Fourier transformation filtered image of (**b**). These images clearly show the stacking sequence and the Zn/Y segregation layers of the 14H-LPSO phase.

6*mm* symmetry and a 2*mm* symmetry indicate a unique 6/*mmm* point group for the 14H-LPSO phase. Figure 4f shows a CBED pattern showing the existence of a mirror plane on (0001). A 6*mm* symmetry and a mirror plane on (0001) further confirm the 6/*mmm* point group for the 14H-LPSO phase. A combination of information derived from these EDPs and the CBED patterns indicates that the 14H-LPSO phase has a point group of 6/*mmm* and a space group of $P6_3/mmc$. Moreover, according to equation (1), the lattice parameter *c* was calculated about 3.68 nm from the first-order Laue zones in Figure 4e, which is consistent with the data deduced from the EDPs aforementioned.

Figure 5a is a HRTEM image of the 14H-LPSO phase recorded with the electron beam parallel to the $\langle 11\bar{2}0\rangle_{\mathrm{LPSO}}$ direction, showing a stacking sequence of AB<u>ABCA</u>CA C<u>ACBA</u>B with a periodicity of 3.68 nm along the [0001] direction, where the underlined characters denote two fcc stacking units. Figure 5b is an HR-STEM image of the 14H-LPSO phase and Figure 5c is a filtered image of Figure 5b, respectively. Similar to the 18R-LPSO phase, the heavier Zn and/or Y atoms distributed periodically at two middle layers of the fcc units, denoted by <u>BC</u>, <u>CB</u>, in the 14H-LPSO phase viewing from the $\langle 11\bar{2}0\rangle_{\mathrm{LPSO}}$ direction (Zhu et al., 2009, 2010). Statistical analysis on 20 EDX spectra shows that the composition of the 14H-LPSO phase is Mg:Zn:Y = (85.6 ± 1.3):(7.1 ± 1.0):(7.3 ± 0.8). Hence, the 14H-LPSO phase is composed of three Mg layers alternating with one fcc stacking unit.

The 18R- and 14H-LPSO phases are the most frequently observed structures in Mg–Zn–Y alloys in an as-cast state (Luo & Zhang, 2000; Itoi et al., 2004; Matsuda et al., 2005; Zhu et al., 2010) and after heat treatment (Kawamura & Yamasaki, 2007; Yoshimoto et al., 2006; Yamasaki et al., 2007; Zhu et al., 2007, 2010). Meanwhile, there is also coexistence of these two LPSO phases in the local domains. Figure 6a shows a medium-magnification TEM image of an intergrown structure 18R- and 14H-LPSO phase in Mg–Zn–Y alloys after heat treatment, combining a very thin Mg slab, about 10 nm in thickness. The intergrowth between these two LPSO phases and Mg platelets

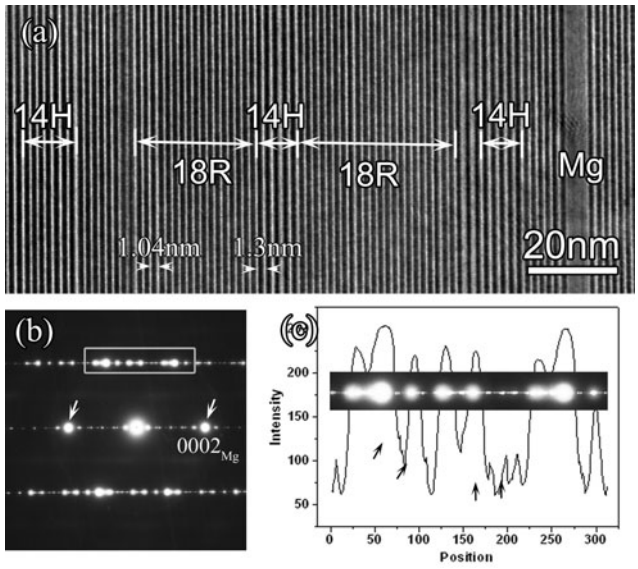

Figure 6. (**a**) A mid-magnification TEM micrograph showing 18R-LPSO and 14H-LPSO phases and Mg platelets alternating with each other; (**b**) the corresponding EDP; (**c**) the intensity profile of reflections among the rectangle denoted in (**b**), the strong peaks arising from the 18R-LPSO phase and the small peaks (shown by arrows) resulting from the 14H-LPSO phase, demonstrates the intergrowth of the two LPSO phases.

can be understood as follows. The lattice parameters *a* of the 18R-LPSO phase and that of the 14H-LPSO phase are essentially equal and proportional to a_α, respectively, allowing an intergrowth with the negligible lattice misfit; in addition, the 18R-LPSO phase shares similar basic stacking layers with the 14H-LPSO phase with the only difference the number of Mg layers between the fcc stacking units (two layers of 18R-LPSO phase and three for the 14H-LPSO phase). Similar intergrown structures have been identified in the ternary Ti–Al–C (Ma et al., 2004), Zr–Al–C (Lin et al., 2006) ceramics and LPSO phases in Mg–Zn–Y alloys (Zhu et al., 2010), which should be a normal phenomenon in the polytypic domains (Lin et al., 2006).

Besides the intergrowth of 18R and 14H-LPSO phases, various number of Mg planes separating the fcc stacking units with two enriched Zn/Y planes were also identified in this Mg–Zn–Y alloy. The *Z*-contrast STEM image of the intergrown structure of different Mg layers distributing Zn/Y layers is illustrated in Figure 7, suggesting that there are two, three, or four Mg layers between two fcc stacking units. If we consider the structures in the left and middle image are 14H- and 18R-LPSO phases, the two Mg layers inserting between the LPSO phases result in stacking faults in the LPSO structures. These stacking faults also are reported in several ternary ceramics due to the insertion of thin layers (Yu et al., 2003; Lin et al., 2006).

Comparing EDPs of the 18R-LPSO (Figs. 2a, 2c, 2d) and 14H-LPSO phases (Figs. 4a–4c), it can be found that the salient feature of the super lattice reflections in the EDPs is almost identical for these two phases. That is, the super lattice spots are relatively sharp on the $(0001)^*$ plane

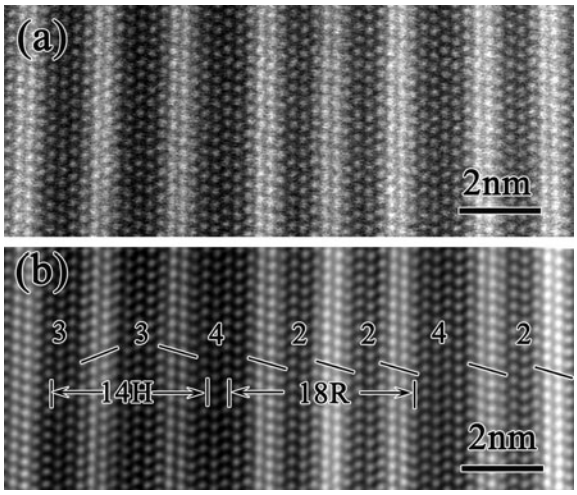

Figure 7. *Z*-contrast STEM image of the intergrown structure of various LPSO phases: (**a**) raw image and (**b**) FFT filtered image. There can be two, three, or four Mg layers separating the fcc stacking sequence.

(Figs. 2a, 4a), while the systematic weak diffuse streaks extend along the c^* direction when the electron beam is parallel to the $[11\bar{2}0]_\alpha$ (Figs. 2c, 4b) and $[1\bar{1}00]_\alpha$ directions (Figs. 2d, 4c). The notable characters of EDPs indicate that there is a comparatively long length of the ordered state in the (0001) basal plane, but a relatively short coherence length of the Zn/Y enriched planes along the c^* direction. This is in good agreement with the *Z*-contrast STEM pictures in Figures 3 and 5–7 that were obtained along the $[11\bar{2}0]_\alpha$ direction, i.e., relatively heavier Zn and/or Y elements concentrated in the adjacent two basal planes and forming a subunit among the LPSO phase. This is similar to the anisotropic features in layered structures, i.e., charge ordering RFe_2O_4 (Zhang et al., 2007*b*) and strontium ordering of $Sr_{0.35}CoO_2$ (Yang et al., 2005).

Conclusions

Microstructural characteristics were investigated in the 18R-LPSO and 14H-LPSO phases using TEM. The point and space groups of the 18R-LPSO phase were determined to be $\bar{3}m$ and $R\bar{3}m$ (or $3m$ and $R3m$), respectively, and the lattice parameter is $a = 1.112$ nm and $c = 4.689$ nm. In contrast, the 14H-LPSO phase has a point group of $6/mmm$ and a space group of $P6_3/mmc$, and the lattice parameter is $a = 1.112$ nm and $c = 3.647$ nm. 18R- and 14H-LPSO phases were identified to form an intergrown structure. Moreover, stacking faults in the LPSO phase resulted from the insertion of additional thin, i.e., only several atomic layers, Mg slabs. The study may lead to a better understanding of the deformation microstructure and properties of LPSO phases in Mg alloys at the atomic level.

Acknowledgment

This work was supported by the National Basic Research Program of China (2009CB623705).

References

Abe, E., Kawamura, Y., Hayashi, K. & Inoue, A. (2002). Long-period ordered structure in a high-strength nanocrystalline Mg-1at%Zn-2at%Y alloy studied by atomic-resolution Z-ontrast STEM. *Acta Mater* **50**, 3845–3857.

Amiya, K., Ohsuna, T. & Inoue, A. (2003). Long-period hexagonal structures in melt-spun $Mg_{97}Ln_2Zn_1$ (Ln = lanthanide metal) alloys. *Mater Trans, JIM* **44**, 2151–2156.

Bae, D., Lee, M., Kim, K., Kim, W. & Kim, D. (2002). Application of quasicrystalline particles as a strengthening phase in Mg-Zn-Y alloys. *J Alloys Compd* **342**, 445–450.

Chino, Y., Mabuchi, M., Hagiwara, S., Iwasaki, H., Yamamoto, A. & Tsubakino, H. (2004). Novel equilibrium two phase Mg alloy with the long-period ordered structure. *Scr Mater* **51**, 711–714.

Hagihara, K., Kinoshita, A., Fukusumi, Y., Yamasaki, M. & Kawamura, Y. (2013). High-temperature compressive deformation behavior of $Mg_{97}Zn_1Y_2$ extruded alloy containing a long-period stacking ordered (LPSO) phase. *Mater Sci Eng A* **560**, 71–79.

Hahn, T., Shmueli, U. & Wilson, A. (1983). *International Tables for Crystallography*. Boston, MA: D. Reidel Publishing Company.

Hirsch, P.B. (1977). *Electron Microscopy of Thin Crystals*. Huntington, NY: Krieger Publishing Company.

Honma, T., Ohkubo, T., Kamado, S. & Hono, K. (2007). Effect of Zn additions on the age-hardening of Mg–2.0Gd–1.2Y–0.2Zr alloys. *Acta Mater* **55**, 4137–4150.

Inoue, A., Kawamura, Y., Matsushita, M., Hayashi, K. & Koike, J. (2001). Novel hexagonal structure and ultrahigh strength of magnesium solid solution in the Mg-Zn-Y system. *J Mater Res* **16**, 1894–1900.

Itoi, T., Seimiya, T., Kawamura, Y. & Hirohashi, M. (2004). Long period stacking structures observed in $Mg_{97}Zn_1Y_2$ alloy. *Scr Mater* **51**, 107–111.

Kawamura, Y., Hayashi, K., Inoue, A. & Masumoto, T. (2001). Rapidly solidified powder metallurgy $Mg_{97}Zn_1Y_2$ alloys with excellent tensile yield strength above 600 MPa. *Mater Trans* **42**, 1172–1176.

Kawamura, Y. & Yamasaki, M. (2007). Formation and mechanical properties of $Mg_{97}Zn_1RE_2$ alloys with long-period stacking ordered structure. *Mater Trans* **48**, 2986–2992.

Lin, Z., Zhuo, M., He, L., Zhou, Y., Li, M. & Wang, J. (2006). Atomic-scale microstructures of $Zr_2Al_3C_4$ and $Zr_3Al_3C_5$ ceramics. *Acta Mater* **54**, 3843–3851.

Luo, Z. & Zhang, S. (2000). High-resolution electron microscopy on the X-$Mg_{12}ZnY$ phase in a high strength Mg-Zn-Zr-Y magnesium alloy. *J Mater Sci Lett* **19**, 813–815.

Ma, X., Zhu, Y., Wang, X. & Zhou, Y. (2004). Microstructural characterization of bulk Ti_3AlC_2 ceramics. *Philos Mag* **84**, 2969–2977.

Matsuda, M., Ii, S., Kawamura, Y., Ikuhara, Y. & Nishida, M. (2005). Variation of long-period stacking order structures in rapidly solidified $Mg_{97}Zn_1Y_2$ alloy. *Mater Sci Eng A* **393**, 269–274.

Matsuura, M., Konno, K., Yoshida, M., Nishijima, M. & Hiraga, K. (2006). Precipitates with peculiar morphology consisting of a disk-shaped amorphous core sandwiched between 14H-typed long period stacking order crystals in a melt-quenched $Mg_{98}Cu_1Y_1$ alloy. *Mater Trans* **47**, 1264–1267.

Mizutani, U., Yamaguchi, T., Tomofuji, T., Yanagi, Y., Itoh, Y., Saitoh, K., Tanaka, N., Matsunami, N. & Ikuta, H. (2009). Factors affecting extreme ultraviolet reflectivity of mo/si multi-

layer films synthesized by superconducting magnetron sputtering. *Jap J Appl Phys* **48**, 25507.

Ono, A., Abe, E., Itoi, T., Hirohashi, M., Yamasaki, M. & Kawamura, Y. (2008). Microstructure evolutions of rapidly-solidified and conventionally-cast $Mg_{97}Zn_1Y_2$ alloys. *Mater Trans* **49**, 990–994.

Pennycook, S. & Jesson, D. (1992). Atomic resolution Z-contrast imaging of interfaces. *Acta Metall Mater* **40**, S149–S159.

Ping, D.H., Hono, K., Kawamura, Y. & Inoue, A. (2002). Local chemistry of a nanocrystalline high-strength $Mg_{97}Y_2Zn_1$ alloy. *Philos Mag Lett* **82**, 543–551.

Shao, X.H., Yang, Z.Q. & Ma, X.L. (2010). Strengthening and toughening mechanisms in Mg-Zn-Y alloy with a long period stacking ordered structure. *Acta Mater* **58**, 4760–4771.

Yamasaki, M., Anan, T., Yoshimoto, S. & Kawamura, Y. (2005). Mechanical properties of warm-extruded Mg-Zn-Gd alloy with coherent 14H long periodic stacking ordered structure precipitate. *Scr Mater* **53**, 799–803.

Yamasaki, M., Sasaki, M., Nishijima, M., Hiraga, K. & Kawamura, Y. (2007). Formation of 14H long period stacking ordered structure and profuse stacking faults in Mg–Zn–Gd alloys during isothermal aging at high temperature. *Acta Mater* **55**, 6798–6805.

Yang, H., Shi, Y., Guo, Y., Liu, X., Xiao, R., Luo, J. & Li, J. (2005). Physical properties, strontium ordering and structural modulation in layered hexagonal $Sr_{0.35}CoO_2$. *Arxiv: cond-mat/* 0503136.

Yoshimoto, S., Yamasaki, M. & Kawamura, Y. (2006). Microstructure and mechanical properties of extruded Mg-Zn-Y alloys with 14H long period ordered structure. *Mater Trans* **47**, 959–965.

Yu, R., Zhan, Q., He, L., Zhou, Y. & Ye, H. (2003). Stacking faults and grain boundaries of Ti_3SiC_2. *Philos Mag Lett* **83**, 325–331.

Zhang, J., Wang, J. & Zhou, Y. (2007*a*). Structure stability of Ti_3AlC_2 in Cu and microstructure evolution of Cu–Ti_3AlC_2 composites. *Acta Mater* **55**, 4381–4390.

Zhang, Y., Yang, H.X., Ma, C., Tian, H.F. & Li, J.Q. (2007*b*). Charge-stripe order in the electronic ferroelectric $LuFe_2O_4$. *Phys Rev Lett* **98**, 247602.

Zhu, Y., Morton, A. & Nie, J. (2007). Characterization of intermetallic phases and planar defects in Mg-Y-Zn alloys. *Mater Sci Forum* **561–565**, 151–154.

Zhu, Y., Morton, A. & Nie, J. (2010). The 18R and 14H long-period stacking ordered structures in Mg-Y-Zn alloys. *Acta Mater* **58**, 2936–2947.

Zhu, Y., Weyland, M., Morton, A., Oh-ishi, K., Hono, K. & Nie, J. (2009). The building block of long-period structures in Mg-RE-Zn alloys. *Scr Mater* **60**, 980–983.